Surface and bulk contributions to the second-harmonic generation in Bi_2Se_3

Hui Shi,[1] Yu Zhang,[1] Mengyu Yao,[2] Fuhao Ji,[1] Dong Qian,[2] Shan Qiao,[3] Y. R. Shen,[1,4,*] and Wei-Tao Liu[1,†]

[1]*Physics Department, State Key Laboratory of Surface Physics, Key Laboratory of Micro and Nano Photonic Structures (MOE), Collaborative Innovation Center of Advanced Microstructures (Nanjing), Fudan University, Shanghai 200433, China*

[2]*Department of Physics and Astronomy, Shanghai Jiao Tong University, Shanghai 200240, China*

[3]*State Key Laboratory of Functional Materials for Information, Shanghai Institute of Microsystem and Information Technology, Shanghai 200050, China*

[4]*Physics Department, University of California at Berkeley, Berkeley, California 94720, USA*

(Received 2 July 2016; revised manuscript received 4 November 2016; published 28 November 2016)

Second harmonic generation (SHG) from three-dimensional topological insulators originates from both surface and bulk, which does not allow probing of surface states unless the measurement can separate the two contributions. In this paper, we used combined measurements of transmitted and reflected SHG from epitaxially grown Bi_2Se_3 thin films of different thickness on BaF_2, and a bulk Bi_2Se_3 crystal, to deduce surface and bulk nonlinear susceptibilities of Bi_2Se_3 separately. We found that the surface contribution to SHG was comparable to that from the bulk of the crystal, but becomes dominant in ultrathin films. In the latter case, contributions from both air/Bi_2Se_3 and Bi_2Se_3/BaF_2 interfaces were significant and exhibited a strong out-of-plane polar ordering. The bulk contribution came mainly from the space charge region (SCR), which was formed by Se vacancies aggregated at the air/Bi_2Se_3 interface; its magnitude can provide an estimate on the field strength in the SCR. Clarification of surface and bulk contributions to SHG can help nonlinear optical techniques be used as a versatile *in situ* probe for topological insulators.

DOI: 10.1103/PhysRevB.94.205307

I. INTRODUCTION

Three-dimensional topological insulators have become a research focus in recent years because of their unique spin-polarized and gapless surface bands [1–5], which are protected by time reversal symmetry, thus highly promising as a platform for spintronics and quantum computing applications [6–9]. Nonetheless, as such surface states are derived from bulk energy bands, it is impossible to physically single out the surface layer to study. The surface response of topological insulators is generally overwhelmed by the bulk response when monitored using conventional transport or linear optical techniques. Second-order nonlinear optical effects, such as second harmonic generation (SHG), can be highly surface specific when applied to materials with inversion symmetry in the bulk [10]. In the presence of a dc field, however, the field-induced second-order nonlinearity in the bulk can be significant [11,12]. This is often the case if a space charge region (SCR) exists in the bulk, for example, near the interface of a semiconductor due to band bending. For the topological insulator Bi_2Se_3 near the air/Bi_2Se_3 interface, Se vacancies tend to migrate from the bulk and accumulate at the interface; the resulting excessive amount of positive surface charges leads to the formation of SCR [13–15]. McIver *et al.* [16] and Hsieh *et al.* [17,18] argued that the SCR contributes as strongly to the reflected SHG as the interface and used SHG to monitor the formation of SCR and spin dynamics, but the surface contribution relative to the SCR bulk contribution is yet to be determined.

In this paper, we would like to separately deduce SHG contributions from the surface and the bulk of Bi_2Se_3. This is possible because the two contributions depend on sample thickness and experimental geometries in different manners. For example, the bulk signal increases with the coherent length of SHG in the material, which is much longer for transmitted than reflected SHG. The surface signal, on the other hand, does not depend on the coherent length. Therefore, by measuring both transmitted and reflected SHG, surface and bulk contributions can be separately deduced [19,20]. This is the approach we adopted in this paper. We measured transmitted and reflected SHG from a Bi_2Se_3 bulk crystal and a set of Bi_2Se_3 thin films of different thickness grown by the molecular beam epitaxial (MBE) on BaF_2 substrates [21]. We found, from reflected SHG, that the surface contribution dominated in very thin films, with strength comparable to that of the bulk contribution from a bulk crystal [16,17]. We also found that, upon formation of the SCR, not only the bulk contribution increased drastically, but the surface contribution also changed significantly, indicating the existence of a direct connection between the surface nonlinear optical susceptibility and the SCR. Since the amount of Se vacancies at the interface was small and would not significantly alter the interfacial structure, the change of the surface nonlinearity presumably was due to that of the surface carrier density. In conventional semiconductors, the second-order nonlinear optical susceptibility becomes sensitive to doping when the Fermi level reaches the less parabolic part of the conduction or valence band. The same reason may apply to surface SHG from Bi_2Se_3 in connection with the surface energy bands. We were also able to obtain the value of the bulk third-order nonlinear susceptibility for the dc-field-induced second-order nonlinearity that can be used to monitor the surface field in the SCR. Moreover, we extracted contribution from the buried Bi_2Se_3/BaF_2 interface that is usually difficult to access [21,22] and found it to have a much stronger out-of-plane polar ordering compared to the air/Bi_2Se_3 interface.

This paper is organized as follows. Section II describes the experimental arrangement. Section III reviews the theory of SHG from a three-layer system and relates the SHG

*yrshen@berkeley.edu
†wtliu@fudan.edu.cn

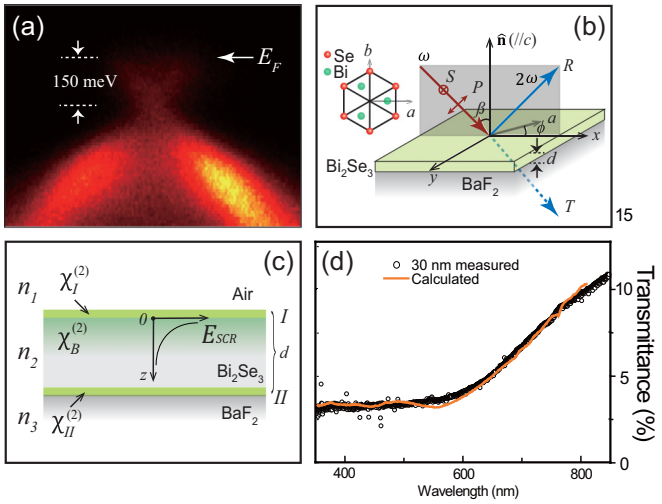

FIG. 1. (a) The ARPES data of a 30 nm thick thin film of Bi_2Se_3. (b) Schematics of the SHG experimental setup and definitions of geometric parameters. Inset shows the lattice coordinates of Bi_2Se_3 with $c \parallel (111)$. (c) Nonlinear susceptibilities, $\chi_I^{(2)}$ $\chi_{II}^{(2)}$ and $\chi_B^{(2)}$, that characterize contributions to SHG from the air/Bi_2Se_3(I) and Bi_2Se_3/BaF_2(II) interfaces, and the bulk Bi_2Se_3, respectively. The last one is dominated by nonlinearity induced by a dc electric field (E_{SCR}) in SCR formed by Se vacancies aggregated at the air/Bi_2Se_3 interface. (d) Measured and calculated linear optical transmission spectra of a 30 nm thick Bi_2Se_3 film on BaF_2.

signals to surface and bulk nonlinear susceptibilities of Bi_2Se_3. Experimental results and values of surface and bulk nonlinear susceptibilities extracted from theoretical fitting as well as other related physical properties of Bi_2Se_3 are presented and discussed in Sec. IV and summarized in Sec. V.

II. EXPERIMENTAL ARRANGEMENT

Bi_2Se_3 (111) films of 10 to 30 nm thick were MBE grown on 1 mm thick barium fluoride (BaF_2) substrates [23]. The zero-gapped surface states of the films were confirmed by the angle-resolved photoemission spectroscopy (ARPES) [1,4] [Fig. 1(a)]. The bulk single crystalline sample was prepared by the Bridgman method [24].

The linear transmission spectra of thin film samples between 350–850 nm were collected by Ocean Optics USB4000 spectrometer at 45° incidence angle. The schematic of the SHG measurement is depicted in Fig. 1(b). We used the 800 nm, 35 fs output from a Ti : sapphire oscillator (Newport, MaiTai SP) as the fundamental beam. It was focused to a spot of 100 μm diameter on the sample surface at 45° incident angle (β) from the surface normal ($\hat{\mathbf{n}}$) with a power density around 0.66 kW/cm^2; no change of the SH signal with time was observed upon such irradiation. The sample could be rotated azimuthally (ϕ) around the surface normal. The SHG output beams were collected simultaneously in both reflected and transmitted directions by two photodetectors (Hamamatsu H8259) after filtering out the fundamental beam; a polarizer before a detector was used to selectively detect the different polarization components of the SH output. The SHG signals from Bi_2Se_3 samples were normalized against that from a z-cut quartz [25,26]. All measurements were performed in air at room temperature.

III. UNDERLYING THEORY

A. SHG from a thin film system

For the air/Bi_2Se_3/BaF_2 [Fig. 1(c)] material we studied, we can model it as a three-layer system. The basic theory of SHG from such a system has been well developed [10,27]. The total SHG signal comes from: (1) the air/Bi_2Se_3 interface (I), (2) the Bi_2Se_3/BaF_2 interface (II), and (3) the bulk of the Bi_2Se_3 film of thickness d (in the case of a Bi_2Se_3 crystal, $d \to \infty$). The SH field $\vec{E}(2\omega)$ in both reflection and transmission can be written as [28]

$$\begin{aligned}\vec{E}_{\rm out}(2\omega) \propto \Big[& \overleftrightarrow{L}(2\omega, z=0)\cdot\overleftrightarrow{\chi}_I^{(2)} : \overleftrightarrow{L}(\omega,0)\overleftrightarrow{L}(\omega,0) \\ & + \overleftrightarrow{L}(2\omega,d)\cdot\overleftrightarrow{\chi}_{II}^{(2)} : \overleftrightarrow{L}(\omega,d)\overleftrightarrow{L}(\omega,d) \\ & + \int_0^d \overleftrightarrow{L}(2\omega,z)\cdot\overleftrightarrow{\chi}_B^{(2)}(z) : \overleftrightarrow{L}(\omega,z)\overleftrightarrow{L}(\omega,z)dz\Big] \\ & \times \vec{E}_{\rm in}(\omega)\vec{E}_{\rm in}(\omega) = \overleftrightarrow{\chi}_{\rm eff}^{(2)} : \vec{E}_{\rm in}(\omega)\vec{E}_{\rm in}(\omega), \end{aligned} \quad (1)$$

where $\overleftrightarrow{\chi}_I^{(2)}$, $\overleftrightarrow{\chi}_{II}^{(2)}$, and $\overleftrightarrow{\chi}_B^{(2)}$ are the surface nonlinear susceptibilities at I and II, and the bulk nonlinear susceptibility in the film bulk, respectively, and $\overleftrightarrow{L}(\Omega,z)$ denotes the tensorial local field factor of frequency Ω at position z (with the air/Bi_2Se_3 interface at $z=0$). The latter relates the local field to the corresponding incoming (ω) or outgoing field (2ω) in the reflected or transmitted direction, including the phase propagating factor. For example, we have $\vec{E}_I(\omega) = \overleftrightarrow{L}(\omega,0)\cdot\vec{E}_{\rm in}(\omega)$, $\vec{E}_{II}(\omega) = \overleftrightarrow{L}(\omega,d)\cdot\vec{E}_{\rm in}(\omega)$, and $\vec{E}_B(\omega,z) = \overleftrightarrow{L}(\omega,z)\cdot\vec{E}_{\rm in}(\omega)$. The SH signal is given by $S(2\omega) \propto |\hat{e}(2\omega)\cdot\overleftrightarrow{\chi}_{\rm eff}^{(2)} : \hat{e}(\omega)\hat{e}(\omega)|^2$, with $\hat{e}(\Omega)$ being the unit polarization vector at Ω.

B. Local field correction factors

The local field (and its derivation) in such a thin film system is well known [28]. In the lab, coordinates (x, y, z) are defined with z along the sample surface normal and x parallel to the beam incident plane. For a beam of frequency Ω with propagation angles of $\beta_j(\Omega)$ in the jth medium (with $j=1$ for air, $j=2$ for Bi_2Se_3, and $j=3$ for BaF_2) characterized by complex refractive indices $\tilde{n}_j(\Omega)$, the local field correction factors $L_{ll}(\Omega,z)$ are [28]

1. For the incoming beam (ω) at z inside the film

$$\begin{aligned} L_{ll}(\omega,z) &= 2\tilde{n}_1 \frac{\tilde{n}_2\cos\delta_{d-z} - \imath\tilde{n}_3\sin\delta_{d-z}}{\epsilon_+\cos\delta_d - \imath\epsilon_-\sin\delta_d} \quad \text{for } l = x,y, \\ &= L_{xx}(\omega,z)\cdot\frac{n_1\cos\beta_1}{n_2\cos\beta_2}\frac{\epsilon_2}{\epsilon'} \quad \text{for } l = z. \end{aligned} \quad (2a)$$

2. For reflected SH beam (2ω) generated by a polarization sheet at z inside the film

$$L_{ll}^{R}(2\omega,z) = 2\bar{n}_1 \frac{\bar{n}_2\cos\delta_{d-z} - \imath\bar{n}_3\sin\delta_{d-z}}{\epsilon_+\cos\delta_d - \imath\epsilon_-\sin\delta_d} \quad \text{for } l = x, y,$$
$$= 2\bar{n}_2 \frac{\bar{n}_3\cos\delta_{d-z} - \imath\bar{n}_2\sin\delta_{d-z}}{\epsilon_+\cos\delta_d - \imath\epsilon_-\sin\delta_d} \cdot \frac{\epsilon_1}{\epsilon'} \quad \text{for } l = z. \tag{2b}$$

3. For transmitted SH beam (2ω) generated by a polarization sheet at z inside the film

$$L_{ll}^{T}(2\omega,z) = 2\bar{n}_3 \frac{\bar{n}_2\cos\delta_z - \imath\bar{n}_1\sin\delta_z}{\epsilon_+\cos\delta_d - \imath\epsilon_-\sin\delta_d} \quad \text{for } l = x,y,$$
$$= 2\bar{n}_2 \frac{\bar{n}_1\cos\delta_z - \imath\bar{n}_2\sin\delta_z}{\epsilon_+\cos\delta_d - \imath\epsilon_-\sin\delta_d} \cdot \frac{\epsilon_3}{\epsilon'} \quad \text{for } l = z. \tag{2c}$$

Note that, for simplicity in writing, we have defined $\bar{n}_j$ differently in different equations: $\bar{n}_j = \frac{\tilde{n}_j}{\cos\beta_j}$ for $l = x$ and z (P-polarized beams), and $\bar{n}_i = \tilde{n}_i\cos\beta_i$ for $l = y$ (S-polarized beams). We have also defined $\delta_z = \frac{n_2\Omega\cos\beta_2}{c}\cdot z$, $\epsilon_+ = \bar{n}_1\bar{n}_2 + \bar{n}_2\bar{n}_3$, $\epsilon_- = \bar{n}_1\bar{n}_3 + \bar{n}_2^2$, and $\epsilon' = \epsilon_2$ in the film, but $\epsilon' = \frac{\epsilon_2(\epsilon_2+5)}{4\epsilon_2+2}$ at both interfaces due to reduced screening [29]. For the two interfaces, local field factors at the air/Bi_2Se_3 boundary are $\overleftrightarrow{L}_I(\Omega) = \overleftrightarrow{L}(\Omega,z=0)$, and those at the Bi_2Se_3/BaF_2 boundary are $\overleftrightarrow{L}_{II}(\Omega) = \overleftrightarrow{L}(\Omega,z=d)$. All these quantities appearing in the expression of $\overleftrightarrow{L}_{ll}(\Omega)$ should be evaluated at frequency Ω. As Eq. (2c) describes the transmitted SH field inside BaF_2, the transmission Fresnel coefficient from BaF_2 to air is to be applied for the field detected in air.

C. Surface and bulk nonlinear susceptibilities of Bi_2Se_3 in the lab coordinates

Crystalline Bi_2Se_3 bulk belongs to the centrosymmetric point group D_{3d} and its second-order nonlinear susceptibility vanishes under electro-dipole approximation. In the presence of an SCR near the air/Bi_2Se_3 interface [Fig. 1(c)], however, a nonnegligible bulk contribution can arise from electric-field-induced nonlinear susceptibility in the SCR [11,12,16,17]. The SCR is formed by accumulation of Se vacancies upon being exposed to air [12,15–17]. Because the interface between Bi_2Se_3 and BaF_2 has only few vacancies or defects [22], we neglect the SCR effect near that interface. If $E_{\rm SCR}(z)\hat{z}$ denotes the dc electric field at z in the SCR, the bulk nonlinear susceptibility at z appears as $\overleftrightarrow{\chi}_B^{(2)}(z) = \overleftrightarrow{\chi}_B^{(3)}\hat{z}E_{\rm SCR}(z)$, where $\overleftrightarrow{\chi}_B^{(3)}$ is the third-order bulk nonlinear susceptibility of Bi_2Se_3. Here, we neglect the bulk electric quadrupole and magnetic dipole contributions in comparison with the SCR contribution [27].

We consider the case that the crystalline Bi_2Se_3 is oriented with the threefold rotation (c) axis along z. The resulting C_{3v} symmetry then leads to the following nonvanishing $\overleftrightarrow{\chi}_B^{(2)}$ elements in the lab coordinates: $\chi_{B,xxx}^{(2)} = -\chi_{B,xyy}^{(2)} = -\chi_{B,yxy}^{(2)} = -\chi_{B,yyx}^{(2)}$, $\chi_{B,yyy}^{(2)} = -\chi_{B,yxx}^{(2)} = -\chi_{B,xyx}^{(2)} = -\chi_{B,xxy}^{(2)}$, $\chi_{B,xxz}^{(2)} = \chi_{B,xzx}^{(2)} = \chi_{B,yyz}^{(2)} = \chi_{B,yzy}^{(2)}$, $\chi_{B,zxx}^{(2)} = \chi_{B,zyy}^{(2)}$, and $\chi_{B,zzz}^{(2)}$ [16]. If the C_{3v} symmetry of Bi_2Se_3 is preserved at the interfaces, then the surface nonlinear susceptibility $\overleftrightarrow{\chi}_S^{(2)}$ ($S = I$ or II) has the same set of nonvanishing elements, i.e., $\chi_{S,xxx}^{(2)} = -\chi_{S,xyy}^{(2)} = -\chi_{S,yxy}^{(2)} = -\chi_{S,yyx}^{(2)}$, $\chi_{S,yyy}^{(2)} = -\chi_{S,yxx}^{(2)} = -\chi_{S,xyx}^{(2)} = -\chi_{S,xxy}^{(2)}$, $\chi_{S,xxz}^{(2)} = \chi_{S,xzx}^{(2)} = \chi_{S,yyz}^{(2)} = \chi_{S,yzy}^{(2)}$, $\chi_{S,zxx}^{(2)} = \chi_{S,zyy}^{(2)}$, and $\chi_{S,zzz}^{(2)}$. Because $\overleftrightarrow{\chi}_B^{(2)}$ and $\overleftrightarrow{\chi}_S^{(2)}$ have the same symmetry, they cannot be distinguished from measurements relying on symmetry only [30].

D. Relations between nonlinear susceptibilities in the lab and crystal coordinates

The crystal coordinates (a,b,c) are defined with c along the threefold symmetric axis of Bi_2Se_3 and a parallel to a mirror plane containing c [Fig. 1(b)]. The lab (x, y, z) and the crystal (a, b, c) coordinates are related by $\hat{a} = \cos\phi\hat{x} + \sin\phi\hat{y}$, $\hat{b} = -\sin\phi\hat{x} + \cos\phi\hat{y}$, and $\hat{c} = \hat{z}$, with ϕ being the azimuthal angle of x from the a-c plane [Fig. 1(b)]. Coordinate transformation connects second-order nonlinear susceptibilities in the lab and crystal coordinates with the expression $\chi_{ijk}^{(2)} = \sum_{lmn}\chi_{lmn}^{(2)}(\hat{i}\cdot\hat{I})(\hat{j}\cdot\hat{m})(\hat{k}\cdot\hat{n})$, where $i,j,k \in \{x,y,z\}$ and $l,m,n \in \{a,b,c\}$. The set of relations for the nonvanishing elements of $\overleftrightarrow{\chi}_S^{(2)}$ ($S = I$ and II) is: $\chi_{S,xxx}^{(2)} = -\chi_{S,xyy}^{(2)} = -\chi_{S,yxy}^{(2)} = -\chi_{S,yyx}^{(2)} = \chi_{S,aaa}^{(2)}\cos3\phi$, $\chi_{S,yyy}^{(2)} = -\chi_{S,yxx}^{(2)} = -\chi_{S,xyx}^{(2)} = -\chi_{S,xxy}^{(2)} = \chi_{S,aaa}^{(2)}\sin3\phi$, $\chi_{S,xxz}^{(2)} = \chi_{S,yyz}^{(2)} = \chi_{S,xzx}^{(2)} = \chi_{S,yzy}^{(2)} = \chi_{S,aac}^{(2)}$, $\chi_{S,zxx}^{(2)} = \chi_{S,zyy}^{(2)} = \chi_{S,caa}^{(2)}$, and $\chi_{S,zzz}^{(2)} = \chi_{S,ccc}^{(2)}$. The same set of relations hold for $\overleftrightarrow{\chi}_B^{(2)}$ [30].

In our experimental study, we focus on the independent, nonvanishing elements $\chi_{S,aaa}^{(2)}$ and $\chi_{S,caa}^{(2)}$ ($S = I$ and II), $\chi_{B,aaa}^{(2)}$ and $\chi_{B,caa}^{(2)}$ that can be more readily deduced from SHG measurements with SSS, SPP (S for the 2ω beam, P for ω), PSS (P for 2ω, S for ω) polarization combinations, where S is along y and P in the x-z plane. The relations between nonlinear susceptibility elements $\chi_{\rm eff}^{(2)}$(SSS), $\chi_{\rm eff}^{(2)}$(SPP), and $\chi_{\rm eff}^{(2)}$(PSS) and the $\overleftrightarrow{\chi}_B^{(2)}$ and $\overleftrightarrow{\chi}_S^{(2)}$ elements in the crystal coordinates can be obtained from Eq. (1). To simplify the expressions, we define

$$\begin{aligned} C_S(\text{SSS}) &= L_{S,yy}(2\omega)L_{S,yy}^2(\omega), \\ C_S(\text{SPP}) &= L_{S,yy}(2\omega)L_{S,xx}^2(\omega)\cos^2\beta_\omega, \\ C_{S,\text{Ani}}(\text{PSS}) &= \pm\cos\beta_{2\omega}L_{S,xx}(2\omega)L_{S,yy}^2(\omega), \\ C_{S,\text{Iso}}(\text{PSS}) &= \sin\beta_{2\omega}L_{S,zz}(2\omega)L_{S,yy}^2(\omega)\,(S = I \text{ and } II), \end{aligned} \tag{3a}$$

with β_ω and $\beta_{2\omega}$ referring to the incident and exit angles of the input fundamental output SH beams, respectively. The $+$ and $-$ signs in $C_{S,\text{Ani}}$(PSS) are for transmitted and reflected SHG, respectively. Note that L_S in Eq. (3a) depends on film thickness. For the bulk, we have $\chi_{B,aaa}^{(2)} = \chi_{B,aaac}^{(3)}E_{\rm SCR}$, and $\chi_{B,caa}^{(2)} = \chi_{B,caac}^{(3)}E_{\rm SCR}$ in terms of nonvanishing $\overleftrightarrow{\chi}_B^{(3)}$

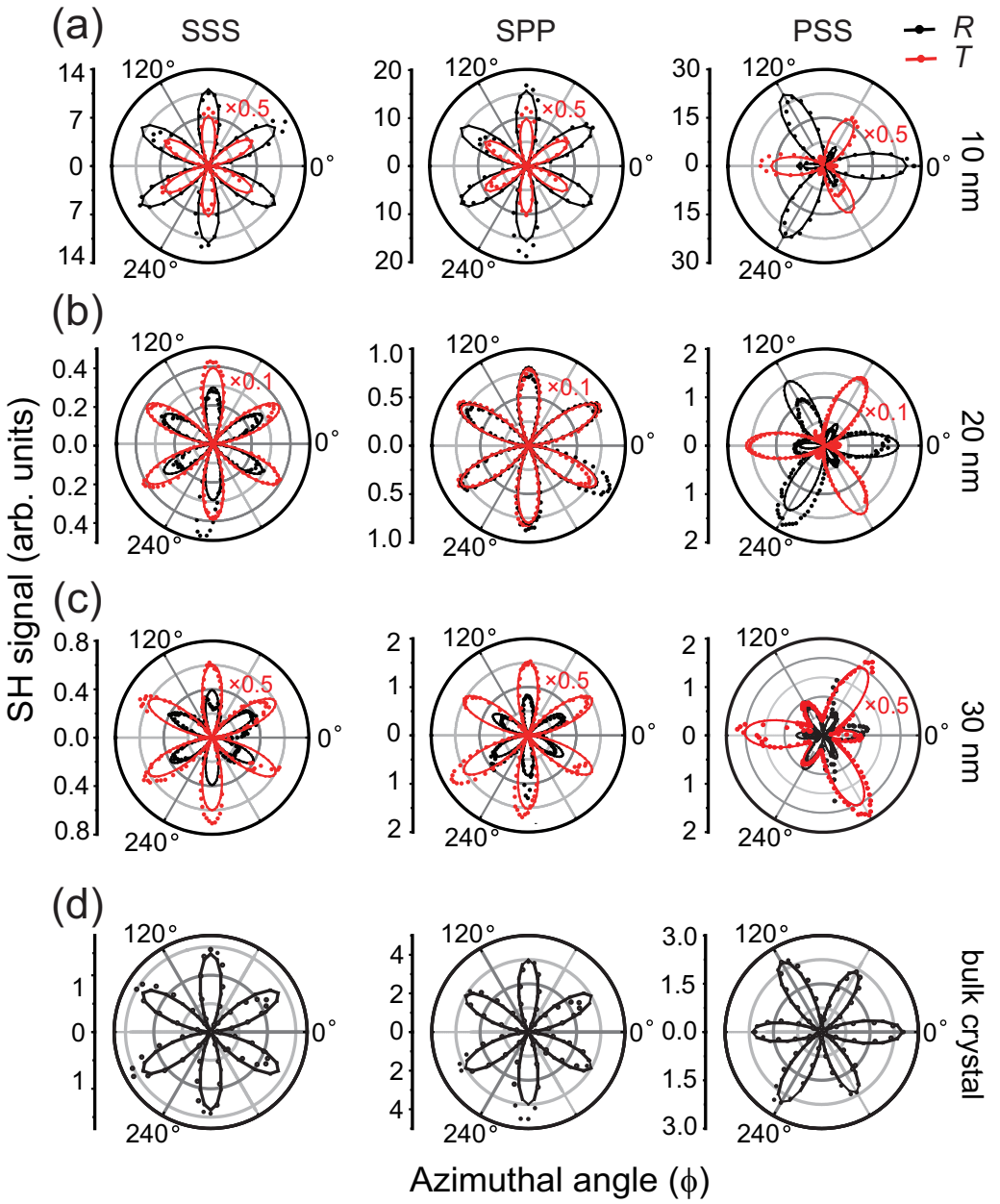

FIG. 2. Azimuthal anisotropy patterns of normalized SHG signals taken from (a) 10 nm, (b) 20 nm, and (c) 30 nm thick Bi_2Se_3 thin films, and (d) the bulk single crystal. The polarization combinations are SSS, SPP, and PSS, respectively (labeled on the top of each column). Black and red dots are the reflected and transmitted signals, respectively. Solid curves are fits by Eq. (3c).

elements [16]. With $E_{\mathrm{SCR}}(z) \equiv E_{\mathrm{SCR}}(0)\varepsilon_{\mathrm{SCR}}(z)$, we define

$$C_B(\mathrm{SSS}) = \int_0^d L_{yy}(2\omega,z)L_{yy}^2(\omega,z)\varepsilon_{\mathrm{SCR}}(z)dz, \quad C_B(\mathrm{SPP}) = \cos^2\beta_\omega \int_0^d L_{yy}(2\omega,z)L_{xx}^2(\omega,z)\varepsilon_{\mathrm{SCR}}(z)dz,$$
$$C_{B,\mathrm{Ani}}(\mathrm{PSS}) = \pm\cos\beta_{2\omega} \int_0^d L_{xx}(2\omega,z)L_{yy}^2(\omega,z)\varepsilon_{\mathrm{SCR}}(z)dz, \quad \text{and} \quad C_{B,\mathrm{Iso}}(\mathrm{PSS}) = \sin\beta_{2\omega} \int_0^d L_{zz}(2\omega,z)L_{yy}^2(\omega,z)\varepsilon_{\mathrm{SCR}}(z)dz. \tag{3b}$$

Note that C_S is dimensionless, while C_B has the unit of length. We then find

$$\chi_{\mathrm{eff}}^{(2)}(\mathrm{SSS}) = \left[C_I(\mathrm{SSS})\chi_{I,aaa}^{(2)} + C_{II}(\mathrm{SSS})\chi_{II,aaa}^{(2)} + C_B(\mathrm{SSS})\chi_{B,aaac}^{(3)}E_{\mathrm{SCR}}(0)\right]\sin 3\phi = \chi_{\mathrm{eff,Ani}}^{(2)}(\mathrm{SSS})\sin 3\phi,$$
$$\chi_{\mathrm{eff}}^{(2)}(\mathrm{SPP}) = \left[C_I(\mathrm{SPP})\chi_{I,aaa}^{(2)} + C_{II}(\mathrm{SPP})\chi_{II,aaa}^{(2)} + C_B(\mathrm{SPP})\chi_{B,aaac}^{(3)}E_{\mathrm{SCR}}(0)\right]\sin 3\phi = \chi_{\mathrm{eff,Ani}}^{(2)}(\mathrm{SPP})\sin 3\phi,$$

$$\chi^{(2)}_{\rm eff}(\mathrm{PSS}) = \left[C_{I,\mathrm{Ani}}(\mathrm{PSS})\chi^{(2)}_{I,aaa} + C_{II,\mathrm{Ani}}(\mathrm{PSS})\chi^{(2)}_{II,aaa} + C_{B,\mathrm{Ani}}(\mathrm{PSS})\chi^{(3)}_{B,aaac}E_{\rm SCR}(0)\right]\cos 3\phi$$
$$+\left[C_{I,\mathrm{Iso}}(\mathrm{PSS})\chi^{(2)}_{I,caa} + C_{II,\mathrm{Iso}}(\mathrm{PSS})\chi^{(2)}_{II,caa} + C_{B,\mathrm{Iso}}(\mathrm{PSS})\chi^{(3)}_{B,caac}E_{\rm SCR}(0)\right] = \chi^{(2)}_{\mathrm{eff,Ani}}(\mathrm{PSS})\cos 3\phi + \chi^{(2)}_{\mathrm{eff,Iso}}(\mathrm{PSS}). \quad (3c)$$

As seen in Eq. (3c), $\chi^{(2)}_{\rm eff}$(SSS), $\chi^{(2)}_{\rm eff}$(SPP) are proportional to $\sin 3\phi$, $\chi^{(2)}_{\rm eff}$(SPP) is composed of an anisotropic term proportional to $\cos 3\phi$ and an isotropic term independent of ϕ. Correspondingly, the SH signals S(SSS) and S(SPP) are proportional to $\sin^2 3\phi$, which exhibits a sixfold symmetry with respect to ϕ, and S(PSS) has a threefold symmetry with respect to ϕ due to interference between the anisotropic ($\propto\cos 3\phi$) and isotropic terms [11,12,16,17].

IV. RESULTS AND DISCUSSION

A. Extraction of nonlinear susceptibility tensor elements

Figure 2 displays the anisotropic patterns of SHG versus azimuthal angle from various samples taken with various polarization combinations (labeled at the head of each column). Figures 2(a)–2(c) are for thin films of 10, 20, and 30 nm, respectively, with black (red) dots referring to the SH signals collected in the reflected (transmitted) directions. Figure 2(d) is for the bulk crystal with SHG in the reflected direction. All signals were normalized against the maximum SSS signal from a z-cut quartz [25,26]. The anisotropy patterns are consistent with Eq. (3c) and with those reported in Refs. [11,12,16,17]. From fitting of the patterns with Eq. (3c) (solid curves in Fig. 2), the anisotropic and isotropic components of the effective surface susceptibility, $\chi^{(2)}_{\rm eff,Ani}$ and $\chi^{(2)}_{\rm eff,Iso}$, for different polarizations can be deduced. The results for different film thicknesses are plotted in Fig. 3 (red circles for transmitted SHG and black squares for reflected SHG; data points at film thickness of 500 nm refer to the bulk crystal). The film thickness in Fig. 3 refers to d in Eqs. (1) and (3). As d decreases, the SH signal from thin films becomes larger than that from the bulk crystal. This is because the local field factors (Sec. IIIB) are greatly enhanced by constructive interference of multiple reflections at the two interfaces.

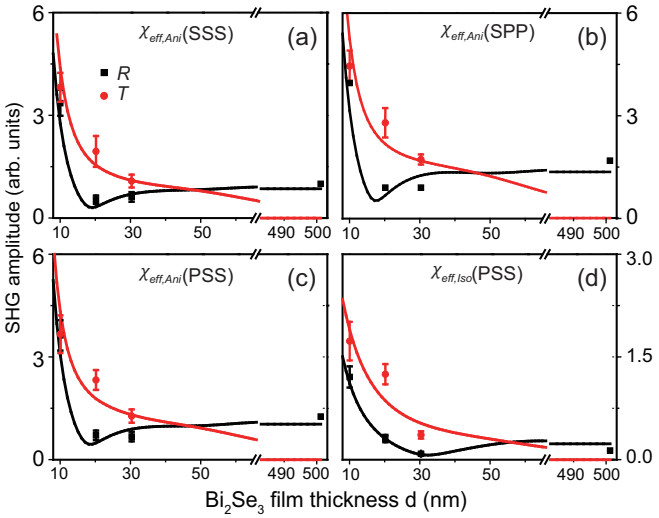

FIG. 3. The film thickness dependence of (a) $|\chi^{(2)}_{\rm eff,Ani}(\mathrm{SSS})|$, (b) $|\chi^{(2)}_{\rm eff,Ani}(\mathrm{SPP})|$, (c) $|\chi^{(2)}_{\rm eff,Ani}(\mathrm{PSS})|$ and (d) $|\chi^{(2)}_{\rm eff,Iso}(\mathrm{PSS})|$. Black and red dots are experimental values of the reflected and transmitted signals, respectively (bulk data are represented by dots at 500 nm). Solid curves are theoretical fits.

We then use Eq. (3c) to fit the data points in Fig. 3, taking the four nonlinear susceptibility elements, $\chi^{(2)}_{S,aaa}$ and $\chi^{(2)}_{S,caa}$ ($S = I$ and II), $\chi^{(2)}_{B0,aaa} \equiv \chi^{(3)}_{B,aaac}E_{\rm SCR}(0)$, and $\chi^{(2)}_{B0,caa} \equiv \chi^{(3)}_{B,caac}E_{\rm SCR}(0)$ in the equation as parameters to be determined. In our calculation, we first calculated the C coefficients in Eqs. (3a) and (3b) versus the film thickness with the help of Eq. (2) and the linear optical constants of bulk Bi_2Se_3. Because reflection high-energy electron diffraction (RHEED) showed that thin films and bulk samples share nearly the same lattice constants, we assumed they have the same linear optical properties as well. To be sure of that, we calculated the transmission spectra of our thin film samples using the bulk refractive index [16] and found good agreement with the experimental data [Fig. 1(d)]. We also adopted the SCR field distribution $\varepsilon_{\rm SCR}(z) \approx e^{-z/t_{\rm SCR}}$ reported in Ref. [15] with $t_{\rm SCR} \approx 4.5$ nm. The calculated magnitudes of various C coefficients versus the film (bulk) thickness d for transmitted and reflected SHG are depicted in Fig. 4. They vary strongly with d, and the field enhancement at small d due to the constructive interference of multiple reflections is clearly seen; also, they approach constants as d goes above 100 nm, at which the contribution from interface II becomes negligible, and the sample can be regarded as semiinfinite.

Knowing the C coefficients, we then calculated $|\chi^{(2)}_{\rm eff,Ani}(\mathrm{SSS})|$, $|\chi^{(2)}_{\rm eff,Ani}(\mathrm{SPP})|$, $|\chi^{(2)}_{\rm eff,Ani}(\mathrm{PSS})|$, and $|\chi^{(2)}_{\rm eff,Iso}(\mathrm{PSS})|$ versus d, using Eq. (3c) and the corresponding nonlinear susceptibility elements in the crystal coordinates as adjustable parameters, to fit data points in Fig. 3. For example, for SSS, we have two sets of data (seven points in total) corresponding to the reflected and transmitted SHG, respectively [Fig. 3(a)], and we fit them simultaneously by the three adjustable parameters, $\chi^{(2)}_{I,aaa}$, $\chi^{(2)}_{II,aaa}$, and $\chi^{(2)}_{B0,aaa}$, using the first equation in Eq. (3c). The best fit is displayed as curves in Fig. 3(a). The same procedure was followed to fit the data for SPP and PSS [Figs. 3(b)–3(d)], respectively. The values of the nonvanishing nonlinear susceptibility elements in the crystal coordinates extracted from different polarization combinations are listed in Table I, showing good consistency in the deduction.

B. The separated surface and bulk contributions

Figure 5 displays the surface-bulk ratio in the reflected direction, defined as $|C_S\chi^{(2)}_S/C_B\chi^{(2)}_{B0}|$ in various cases. It shows that, for the semiinfinite crystal, the anisotropic surface and bulk contributions are comparable

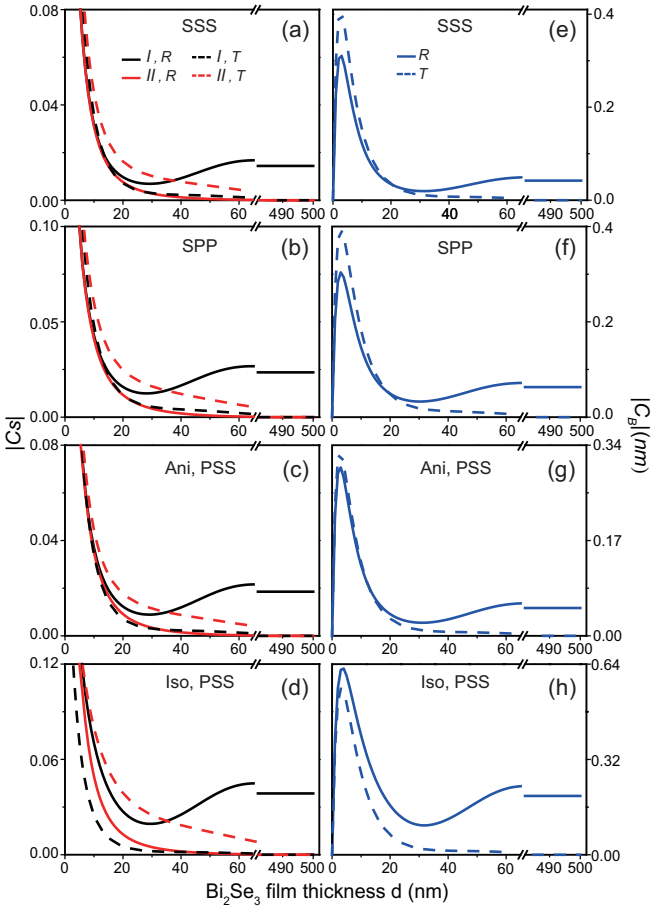

FIG. 4. Magnitudes of calculated local field factors: (a) $|C_S(\mathrm{SSS})|$, (b) $|C_S(\mathrm{SPP})|$, (c) $|C_{S,\mathrm{Ani}}(\mathrm{PSS})|$, and (d) $|C_{S,\mathrm{Iso}}(\mathrm{PSS})|$; (e) $|C_B(\mathrm{SSS})|$, (f) $|C_B(\mathrm{SPP})|$, (g) $|C_{B,\mathrm{Ani}}(\mathrm{PSS})|$, and (h) $|C_{B,\mathrm{Iso}}(\mathrm{PSS})|$, for reflected (solid curves) and transmitted (dashed curves) signals versus the film thickness. In panels (a)–(d), black curves are for the air/Bi_2Se_3 interface (I), red curves are for the Bi_2Se_3/BaF_2 interface (II).

($|C_S\chi^{(2)}_{S,aaa}/C_B\chi^{(2)}_{B0,aaa}| \approx 1$) [Fig. 5(a)]. The isotropic surface contribution, on the other hand, is in general larger than that of the bulk, especially for very thin films.

For films thinner than 50 nm, the SH contribution from interface II is detectable [Fig. 5(b)]. This buried interface is difficult to access by usual means [21,22], but it is part of the topological surface of Bi_2Se_3 and should contribute to the transport properties of the Bi_2Se_3/BaF_2 system. We

TABLE I. Nonlinear optical susceptibility tensor elements extracted from different polarization combinations. The uncertainty is ~10% in average.

	$\lvert\chi^{(2)}_{j,aaa}\rvert(10^{-18}\,\mathrm{m^2/V})$			$\lvert\chi^{(2)}_{j,caa}\rvert(10^{-18}\,\mathrm{m^2/V})$		
j	I	II	$B0\,(\mathrm{nm^{-1}})$	I	II	$B0\,(\mathrm{nm^{-1}})$
SSS	4.7	3.4	1.6			
SPP	4.7	3.4	1.6			
PSS	4.5	3.5	1.5	0.14	0.54	0.009

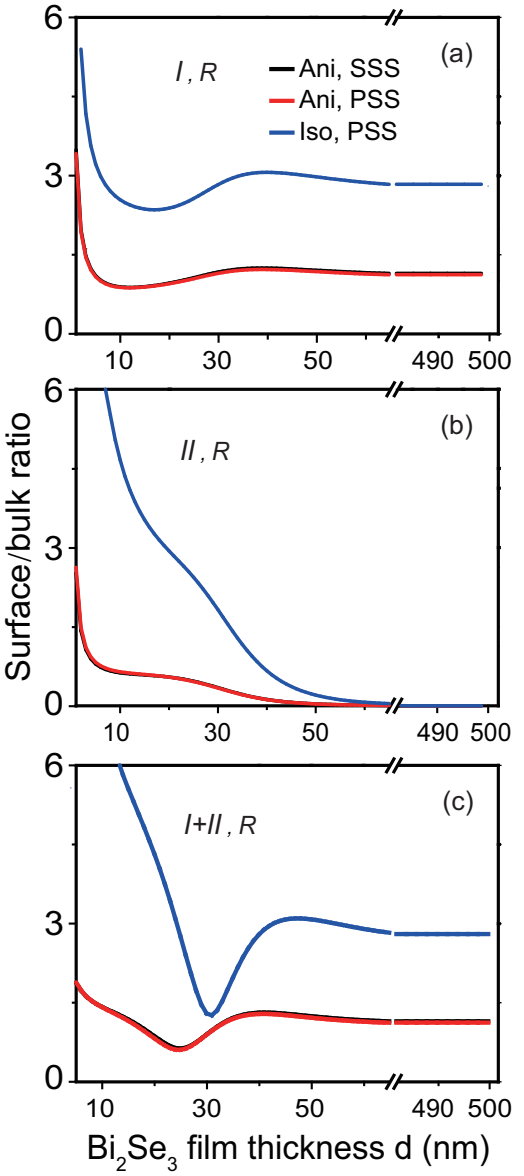

FIG. 5. The ratio between different surface and bulk susceptibility tensor elements: (a) interface I versus the bulk, (b) interface II versus the bulk, and (c) total interfaces $I + II$ versus the bulk.

found that $|\chi^{(2)}_{II,aaa}| \sim |\chi^{(2)}_{I,aaa}|$ (Table I), while $|\chi^{(2)}_{II,caa}|$ is much larger than $|\chi^{(2)}_{I,caa}|$. Since $\chi^{(2)}_{caa}$ and $\chi^{(2)}_{aaa}$ are measures of the out-of-plane and in-plane nonlinear polarizabilities, respectively, the above result indicates that the Bi_2Se_3/BaF_2 interface has an appreciably stronger out-of-plane polar ordering compared to air/Bi_2Se_3. Our result is in line with the previous transmission electron microscopy (TEM) study showing that the Bi_2Se_3/BaF_2 interface is highly ordered with an atomically sharp boundary with very few defects [22]. It is also possible that lattice mismatch may slightly change the out-of-plane bond length and affect the interfacial polarity, leading to the observed change in nonlinear susceptibility.

For films thicker than 50 nm, the SHG signal is predominantly from interface I and its adjacent bulk SCR. The SCR is believed to originate from accumulation of Se

vacancies at the Bi_2Se_3 surface upon exposure to air [16,17]. In Ref. [17], the reflected anisotropic SHG signal from a cleaved bulk Bi_2Se_3 crystal was found to gradually increased by about two times after cleavage in air [13–15,31]. This change is not only from the bulk due to formation of SCR, but also from the surface. Right after cleavage ($t = 0$), there is no SCR in the absence of Se vacancy; so $\overleftrightarrow{\chi}^{(2)}_B(t = 0)| = 0$, and the SH signal for the SSS polarization is $S(\mathrm{SSS})|_{t=0} \propto |C_I(\mathrm{SSS})\chi^{(2)}_{I,aaa}(t = 0)|^2$. After stabilized in air ($t = \infty$), the SCR is formed, and the signal becomes $S(\mathrm{SSS})|_{t=\infty} \propto |C_I(\mathrm{SSS})\chi^{(2)}_{I,aaa}(t = \infty) + C_B(\mathrm{SSS})\chi^{(2)}_{B0,aaa}(t = \infty)|^2$. Our measurements were carried out at $t = \infty$, and we found that $|C_I(\mathrm{SSS})\chi^{(2)}_{I,aaa}(t = \infty)|/|C_B(\mathrm{SSS})\chi^{(2)}_{B0,aaa}(t = \infty)| \approx 1.17$. Knowing $S(\mathrm{SSS})|_{t=\infty} \sim 2S(\mathrm{SSS})|_{t=0}$ from Ref. [17], we obtained $|\chi^{(2)}_{I,aaa}(t = \infty)/\chi^{(2)}_{I,aaa}(t = 0)| \approx 4$. Similarly, we found $|\chi^{(2)}_{I,caa}(t = \infty)/\chi^{(2)}_{I,caa}(t = 0)| \approx 4$. Obviously, formation of Se vacancies has a significant effect on the surface nonlinearity of Bi_2Se_3. It is known that carrier contribution to the nonlinear susceptibility of conventional semiconductors increases when the Fermi level moves toward the nonparabolic region of the conduction or valence band [32,33]. Thus, surface doping of Bi_2Se_3 may indeed lead to appreciable change of its surface nonlinear susceptibility. Further theoretical and experimental studies of how surface doping affects surface nonlinear susceptibility in relation to changes of surface band structure and surface carrier density will be useful.

Finally, we can derive values of Bi_2Se_3 susceptibilities using quartz as a reference [25,26]. In our experiment, the input photon energy was 1.5 eV, and the outgoing photon energy was 3.0 eV, both being well above the bulk bandgap. We found $|\chi^{(2)}_{I,aaa}| \sim 4.6 \times 10^{-18}\,\mathrm{m^2/V}$ and $|\chi^{(2)}_{I,caa}| \sim 1.4 \times 10^{-19}\,\mathrm{m^2/V}$ for the air/Bi_2Se_3 interface. They are comparable to $|\chi^{(2)}_S| \sim 10^{-18} - 10^{-19}\,\mathrm{m^2/V}$ for a monolayer of rhodamine dye molecules at the lowest electronic resonance [20,34,35]. For the bulk nonlinear susceptibilities, we found $|\chi^{(2)}_{B0,aaa}| \sim 1.6 \times 10^{-9}\,\mathrm{m/V}$ and $|\chi^{(2)}_{B0,caa}| \sim 9 \times 10^{-12}\,\mathrm{m/V}$. If we take $E_{\mathrm{SCR}}(0) \sim 0.03\frac{\mathrm{V}}{\mathrm{nm}}$ as in Ref. [15], we obtained $|\chi^{(3)}_{B,aaac}| \sim 5 \times 10^{-17}\,\mathrm{m^2/V^2}$ and $|\chi^{(3)}_{B,caac}| \sim 3 \times 10^{-19}\,\mathrm{m^2/V^2}$ for Bi_2Se_3. These values are of the same order of magnitude as those of the corresponding nonlinear susceptibilities of Si ($\sim 10^{-19}\,\mathrm{m^2/V^2}$) and Ge ($\sim 10^{-18}\,\mathrm{m^2/V^2}$), both with input wavelength at ~1000 nm [32,33,36,37]. With $|\chi^{(3)}_B|$ determined, in principle, we can then use SHG as an *in situ* and quantitative probe of the SCR electric field in Bi_2Se_3.

V. CONCLUSION

To summarize, we separately determined the surface and bulk contributions to SHG from MBE grown Bi_2Se_3 thin films on BaF_2 and a bulk Bi_2Se_3 crystal. We found that the surface contribution was comparable to the bulk in the crystal, but dominated in very thin films. Being able to distinguish surface and bulk contributions, SHG could be used to investigate the effect of surface doping on both bulk and surface structures of topological insulators, including that of the buried sample/substrate interface which is usually hard to access by other means. The technique could serve as a versatile tool for studying topological insulators if a microscopic theory on their surface and bulk nonlinearities were available.

ACKNOWLEDGMENTS

This paper was supported by the National Natural Science Foundation of China, the National Basic Research Program of China under Grant Agreements 11374065, 2012CB921400, 2016YFA0300902, 11622429, 11574201, and 11304338. Y.R.S. also acknowledges support from the Director, Office of Science, Office of Basic Energy Sciences, Materials Sciences and Engineering Division, of the US Department of Energy under Contract No. DE-AC03-76SF00098.

[1] D. Hsieh, D. Qian, L. Wray, Y. Xia, Y. S. Hor, R. J. Cava, and M. Z. Hasan, Nature (London) **452**, 970 (2008).
[2] M. Z. Hasan and C. L. Kane, Rev. Mod. Phys. **82**, 3045 (2010).
[3] J. E. Moore, Nature (London) **464**, 194 (2010).
[4] X. L. Qi and S. C. Zhang, Rev. Mod. Phys. **83**, 1057 (2011).
[5] C. L. Kane and E. J. Mele, Phys. Rev. Lett. **95**, 146802 (2005).
[6] P. Wei, Z. Wang, X. Liu, V. Aji, and J. Shi, Phys. Rev. B **85**, 201402(R) (2012).
[7] H. Yuan, H. Liu, H. Shimotani, H. Guo, M. Chen, Q. K. Xue, and Y. Iwasa, Nano Lett. **11**, 2601 (2011).
[8] H. Steinberg, D. R. Gardner, Y. S. Lee, and P. Jarillo-Herrero, Nano Lett. **10**, 5032 (2010).
[9] X. L. Qi, T. L. Hughes, and S. C. Zhang, Phys. Rev. B **78**, 195424 (2008).
[10] Y. R. Shen, *Principles of Nonlinear Optics* (Wiley-Interscience, New York, 1984).
[11] Y. D. Glinka, S. Babakiray, T. A. Johnson, M. B. Holcomb, and D. Lederman, Phys. Rev. B **91**, 195307 (2015).
[12] C. Xu, A. Hewitt, J. Wang, T. Guan, J. Boltersdorf, P. A. Maggard, D. B. Dougherty, and K. Gundogdu, J Appl. Phys. **116**, 043519 (2014).
[13] C. E. ViolBarbosa, C. Shekhar, B. Yan, S. Ouardi, E. Ikenaga, G. H. Fecher, and C. Felser, Phys. Rev. B **88**, 195128 (2013).
[14] H. M. Benia, C. Lin, K. Kern, and C. R. Ast, Phys. Rev. Lett. **107**, 177602 (2011).
[15] M. Bianchi, D. Guan, S. Bao, J. Mi, B. B. Iversen, P. D. C. King, and P. Hofmann, Nat. Commun. **1**, 128 (2010).
[16] J. W. McIver, D. Hsieh, S. G. Drapcho, D. H. Torchinsky, D. R. Gardner, Y. S. Lee, and N. Gedik, Phys. Rev. B **86**, 035327 (2012).
[17] D. Hsieh, J. W. McIver, D. H. Torchinsky, D. R. Gardner, Y. S. Lee, and N. Gedik, Phys. Rev. Lett. **106**, 057401 (2011).

[18] D. Hsieh, F. Mahmood, J. W. McIver, D. R. Gardner, Y. S. Lee, and N. Gedik, Phys. Rev. Lett. **107**, 077401 (2011).
[19] Y. R. Shen, J Phys. Chem. C **116**, 15505 (2012).
[20] X. Wei, S. C. Hong, A. I. Lvovsky, H. Held, and Y. R. Shen, J. Phys. Chem. B **104**, 3349 (2000).
[21] O. Caha, A. Dubroka, J. Humlíček, V. Holý, H. Steiner, M. Ul-Hassan, J. Sánchez-Barriga, O. Rader, T. N. Stanislavchuk, A. A. Sirenko, G. Bauer, and G. Springholz, Cryst. Growth Des. **13**, 3365 (2013).
[22] B. A. Assaf, F. Katmis, P. Wei, B. Satpati, Z. Zhang, S. P. Bennett, V. G. Harris, J. S. Moodera, and D. Heiman, Appl. Phys. Lett. **105**, 102108 (2014).
[23] X. Chen, X. C. Ma, K. He, J. F. Jia, and Q. K. Xue, Adv. Mater. **23**, 1162 (2011).
[24] P. Rudolph, *Handbook of Crystal Growth: Bulk Crystal Growth* (Elsevier Science, Amsterdam, 2014).
[25] W.-T. Liu and Y. R. Shen, Phys. Rev. Lett. **101**, 016101 (2008).
[26] W.-T. Liu and Y. R. Shen, Phys. Rev. B **78**, 024302 (2008).
[27] Y. R. Shen, Annu. Rev. Phys. Chem. **40**, 327 (1989).
[28] D. Wilk, D. Johannsmann, C. Stanners, and Y. R. Shen, Phys. Rev. B **51**, 10057 (1995).
[29] X. Zhuang, P. B. Miranda, D. Kim, and Y. R. Shen, Phys. Rev. B **59**, 12632 (1999).
[30] W. Liu and Y. R. Shen, Ann. Phys. (Berlin) **523**, 101 (2011).
[31] D. Hsieh, Y. Xia, D. Qian, L. Wray, F. Meier, J. H. Dil, J. Osterwalder, L. Patthey, A. V. Fedorov, H. Lin, A. Bansil, D. Grauer, Y. S. Hor, R. J. Cava, and M. Z. Hasan, Phys. Rev. Lett. **103**, 146401 (2009).
[32] J. J. Wynne, Phys. Rev. **178**, 1295 (1969).
[33] S. S. Jha and N. Bloembergen, Phys. Rev. **171**, 891 (1968).
[34] S. M. Anderson, N. Tancogne-Dejean, B. S. Mendoza, and V. Véniard, Phys. Rev. B **91**, 075302 (2015).
[35] M. B. Raschke, M. Hayashi, S. H. Lin, and Y. R. Shen, Chem. Phys. Lett. **359**, 367 (2002).
[36] S. Y. Yuen and P. A. Wolff, Appl. Phys. Lett. **40**, 457 (1982).
[37] R. W. Boyd, Z. Shi, and I. De Leon, Opt. Commun. **326**, 74 (2014).